2015

Young's modulus of [111] germanium nanowires

M. Maksud
Virginia Commonwealth University, maksudm@vcu.edu

J. Yoo
Center for Integrated Nanotechnologies

C. T. Harris
Center for Integrated Nanotechnologies

N. K. R. Palapati
Virginia Commonwealth University, palapatinkr@vcu.edu

A. Subramanian
Virginia Commonwealth University, asubramanian@vcu.edu

Young's modulus of [111] germanium nanowires

M. Maksud,[1] J. Yoo,[2] C. T. Harris,[3] N. K. R. Palapati,[1] and A. Subramanian[1,a]
[1]*Department of Mechanical and Nuclear Engineering, Virginia Commonwealth University, Richmond, Virginia 23284, USA*
[2]*Center for Integrated Nanotechnologies, Los Alamos National Laboratory, Los Alamos, New Mexico 87545, USA*
[3]*Center for Integrated Nanotechnologies, Sandia National Laboratories, Albuquerque, New Mexico 87185, USA*

(Received 25 August 2015; accepted 20 October 2015; published online 2 November 2015)

This paper reports a diameter-independent Young's modulus of 91.9 ± 8.2 GPa for [111] Germanium nanowires (Ge NWs). When the surface oxide layer is accounted for using a core-shell NW approximation, the YM of the Ge core approaches a near theoretical value of 147.6 ± 23.4 GPa. The ultimate strength of a NW device was measured at 10.9 GPa, which represents a very high experimental-to-theoretical strength ratio of ~75%. With increasing interest in this material system as a high-capacity lithium-ion battery anode, the presented data provide inputs that are essential in predicting its lithiation-induced stress fields and fracture behavior. [http://dx.doi.org/10.1063/1.4935060]

Nanostructured, lithium-alloying electrodes provide a promising pathway towards substantively increasing the energy density in lithium-ion (Li-ion) battery anodes beyond the capabilities of graphite, which has a theoretical capacity of 372 mAh/g and remains the predominant choice in current commercial batteries. One-dimensional silicon and germanium have attracted the most interest among this family of lithium alloying material systems.[1–4] Interest in silicon nanowires (NWs)[1] has emerged from their ability to reversibly store lithium at gravimetric capacities approaching their theoretical value (of 3579 mAh/g), which is the highest among all known electrode materials. On the other hand, germanium NWs[2–4] have attracted increasing attention due to their superior rate capabilities even though their gravimetric capacity of 1384 mAh/g is lower than that of Si. This improvement in rate or power capability arises from their superior metrics in terms of Li^+ diffusivity (~400× larger than Si) and electrical conductivity (10 000× larger than Si).[3–6] Another favorable attribute associated with crystalline Ge relates to its enhanced fracture resistance towards electrochemical lithiation as compared to crystalline Si.[7]

While nanostructuring of these materials in a one-dimensional form offers directional strain relaxation along their longitudinal axis, an accurate understanding of their mechanical properties is still essential due to the large volume changes during the reversible lithium alloying process. The Young's Modulus (YM) is a critical parameter in the development of stress-fields and fracture within a battery electrode during lithiation, and hence, its quantification is important.[8] For instance, Ge undergoes a 300% volume change upon full lithiation[4] and its YM plays a key role in its mechanical stability during this volume expansion process. In previous studies, YM values of 106 ± 19 GPa[9] and 112 ± 43 GPa[10] were reported for NWs synthesized in the [110] and [112] directions, respectively. Here, we present YM measurements from Ge NWs grown in the [111] direction. These measurements were performed on single NW, doubly clamped devices using an atomic force microscopy (AFM) based, three-point bending technique.[10–13] In addition, the ultimate strength of these nanowires was estimated from an experiment involving brittle fracture in one of the tested NW devices.

[a]Author to whom correspondence should be addressed. Electronic mail: asubramanian@vcu.edu.

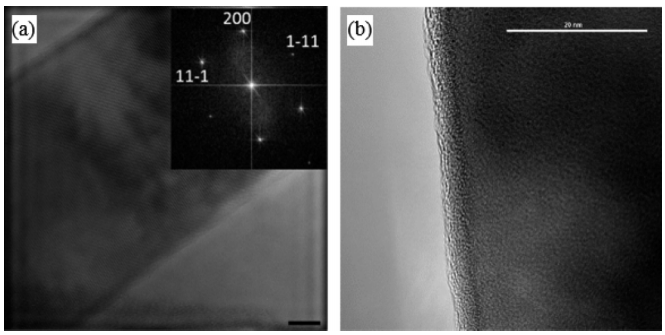

FIG. 1. (a) HR-TEM image of [111] Ge NW with the electron diffraction pattern shown in the inset. (b) An image showing the amorphous oxide layer, with a nominal thickness of ~3 nm, on the NW surface. The scale bars in panels "a" and "b" measure 5 nm and 20 nm, respectively.

In this effort, Au-catalyzed Ge NWs, which are shown in Fig. 1, were grown by vapor-liquid-solid mechanism via low-pressure chemical vapor deposition (LPCVD). Au nanoparticles (NPs) with diameters of 30 nm were dispersed on pre-cleaned Ge (111) substrates. To enhance the adhesion of Au NPs, (3-Aminopropyl)triethoxysilane was coated onto the Ge substrates before the dispersion of Au NPs. 30% GeH_4 diluted in H_2 was employed as the gaseous precursor for the NW synthesis step. This Ge NW growth process consisted of two stages: nucleation (2 min) and elongation (10 min), respectively. The growth temperature and chamber pressure for the nucleation stage were maintained at 350 °C and 2 Torr, respectively. The elongation stage follows the nucleation stage with a growth temperature of 265 °C and did not involve changes in other growth parameters. The NWs tested in this effort ranged in radius and length between ~10 and 20 nm and ~1-5 μm, respectively.

The synthesized Ge NWs were harvested from the substrate and suspended in ethanol using ultrasonication. The NWs in solution were then captured across the surface of opposing gold nanoelectrode pairs using dielectrophoresis (DEP) (Fig. 2(a)).[14–17] The gold nanoelectrodes were defined as a part of an array of devices on silicon substrates. The DEP parameters such as voltage, time, and frequency were optimized to yield either a single or a few non-overlapping nanowires at each device location in the electrode array. From among these devices, the locations containing only a single NW were selected for further testing. Next, the nanowires at these selected locations were clamped at their distal ends from the top-side using electron beam induced deposition (EBID) of platinum (Fig. 2(a)). This results in the formation of doubly clamped Ge NW beams, which are conducive for nanomechanical characterization using the AFM. Further information on the chip nanofabrication and DEP nanoassembly processes can be found elsewhere in our past reports.[15–17]

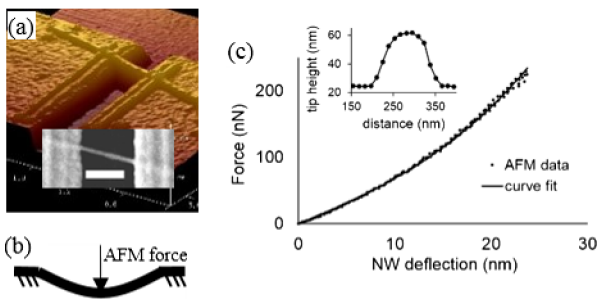

FIG. 2. (a) A 3D, tapping mode AFM image of a NW device, which is clamped on the top-side with EBID Pt. The inset shows a SEM image of the NW (scale bar = 300 nm). (b) A schematic illustration of the AFM-based, three point bending test and the NW deformation in the doubly clamped mode. The arrow indicates the force exerted by the AFM tip. (c) The force vs. displacement plot of the NW. The NW height trace, which was obtained from a separate tapping mode scan, is shown in the inset.

The static force *vs.* deflection (F-d) curves of the Ge NW beams were acquired using an AFM based three-point bending method.[10–13] This measurement was carried out at room temperature (~298 K) and in air (atmospheric conditions). In this experiment, the nanowire beams, which are anchored at their terminal ends, are subjected to transverse loads at their mid-lengths using the force exerted by an AFM tip. This is accomplished by pushing the sample upwards against the tip. During this process, signals from the AFM photodetector and from the piezo-actuator controlling the sample stage are monitored to obtain the tip deflection (δ_{tip}) and stage displacement (δ_{stage}), respectively. From these variables, the tip force acting on the NW is calculated as $F_{NW} = k_{tip} * \delta_{tip}$, where the spring constant of the AFM cantilever (k_{tip}) is obtained using Sader's resonance damping method,[18] and the NW deflection is calculated as $\delta_{NW} = \delta_{stage} - \delta_{tip}$. The resulting F-d relationship is used to extract the YM of the NW sample. The F-d curve for the NW sample of Fig. 2(a) is shown in panel "c" of this image.

As seen in Fig. 2(c), the deflection of the NW increases almost linearly with the applied force in the small deformation region, which extends up to a characteristic value approaching the radius of the wire. This near-linear relationship indicates that the NW is subjected to bending in this portion of the F-d curve. At larger NW deformations, the F-d curve is non-linear. The non-linearity emerges from the one-dimensional nature of the nanobeam, which results in a combination of bending and tensile stretching at large deformations.[10,19] This non-linear F-d behavior in one-dimensional nano-beams can be expressed using the following model:[10,13]

$$F_{NW} = \frac{192EI}{L^3}\delta_{NW} f(\alpha), \tag{1}$$

where $f(\alpha) = \frac{\alpha}{48-192\tanh(\sqrt{\alpha}/4)/\sqrt{\alpha}}$, $\alpha = \frac{6\epsilon(140+\epsilon)}{350+3\epsilon}$, and $\epsilon = \left(\frac{2\delta_{NW}}{R_{NW}}\right)^2$. Also, E, I ($= \pi R_{NW}^4/4$), L, and R_{NW} represent the YM, moment of inertia, NW beam length, and NW radius, respectively. In our experiments, the NW beam length and radius were estimated from tapping-mode AFM height plots (inset of Fig. 2(c)) and from SEM images, respectively. By fitting the observed experimental data to this analytical model, the NW YM (i.e., the unknown parameter) is extracted. For the Ge NWs tested in this work, the non-linear relationship given by Eq. (1) was found to accurately describe the observed F-d behavior, which can be clearly seen from the data shown in Fig. 2(c). For this NW device with a radius of 15 nm, the YM was calculated as 89.4 GPa.

A total of 7 [111] Ge NW samples were tested, and the average value of their YM was obtained as 91.9 GPa (with 95% confidence limits of ±8.2 GPa). Table I lists the NW dimensions (i.e., the radius/length) and the measured YM for these 7 samples. The variations in NW beam length (L) arises from the following factors: (a) the differences in electrode designs within the array, where the inter-electrode design spacing was fixed at 400 nm at one-half of the locations and at 800 nm at the rest of the locations, and (b) the differences in orientation of the assembled NWs with respect to the electrode gaps. The YM values are also plotted as a function of NW radius in Fig. 3. This plot reveals that, within the measured range of radii, the YM is independent of the NW radius and agrees with past measurements involving Ge NWs.[9,10] These past experiments have reported YM values of 106 ± 19 GPa and 112 ± 43 GPa for single crystal Ge NWs oriented along the [110] and [112] directions, respectively.[9,10] Our results, taken together with previously published data, point to the dependence of YM on the crystal orientation, as would be expected. It is important to note

TABLE I. The measured YM values and dimensions for the NW samples.

NW sample	Radius (R_{NW}, nm)	Length (L, nm)	YM (GPa)
1	17	389	109.6
2	18.2	400	96
3	18.8	393	84.8
4	15	474	89.4
5	16.2	447	75.9
6	12.5	800	100.4
7	12.5	802	87.4

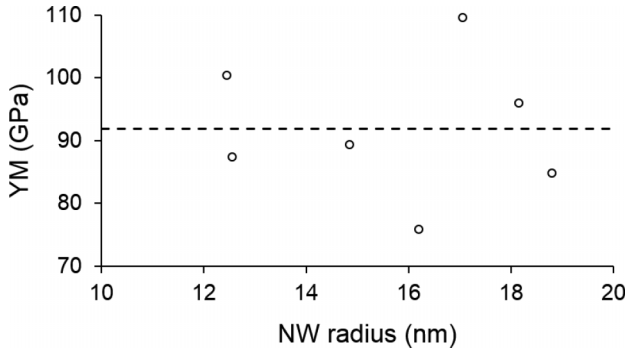

FIG. 3. YM vs. radius plot for 7 NW samples. The average value for the YM is shown using the dotted line.

that the theoretical values for YM in Ge crystals are estimated to be 103, 138, and 155 GPa for the [100], [110], and [111] directions, respectively.[20,21] These values have also been consistent with density-functional theory calculations for Ge NWs when their diameters exceeded 2 nm.[22]

The measured YM value is lower than the theoretical estimate of 155 GPa[22] for [111] NW crystals. We attribute this difference to the presence of an amorphous and much softer germanium oxide layer on the surface of these wires. The existence of such an oxide is evidenced by the TEM images presented previously (Fig. 1). The nominal thickness of the oxide layer was measured from these micrographs and was determined to be ~3 nm. To estimate the intrinsic modulus of the Ge core, we employed a core-shell model[23] for these NWs, using an approximate thickness of 3 nm for the oxide shell layer. Using this approach, the YM of the Ge core can be calculated as $E_{Ge} = (EI - E_{ox}I_{ox})/I_{Ge}$,[23] where E_{ox}, I_{ox}, and I_{Ge} represent the YM of the oxide shell, moment inertia of the oxide shell and the moment of inertia of the Ge core, respectively. Assuming an oxide thickness of 3 nm and an oxide YM of 53 GPa,[24] the intrinsic YM of the [111] Ge NWs is obtained as 147.6 ± 23.4 GPa. It is important to note that the value for the oxide YM, which has been used here and has been cited in the past with the [112] Ge NW[10] system, is obtained from cylindrical specimens with millimeter-scale diameters and represents the best available estimate for the surface oxide layer. The YM value, which is obtained after accounting for the oxide layer, is very near to the theoretical estimate of 155 GPa[22] for this crystal direction and hence supports our argument that the observation of a lower YM in our NWs is due to its surface oxide layer.

The fracture behavior of one of the NW samples provides additional insights into the ultimate strength of this material system. The AFM trace-retrace curve (i.e., the raw data from tip deflection/stage movement signals) representing the loading and unloading behaviors of the NW sample and the resulting F-d curve prior to fracture are shown in Fig. 4. From this figure, it is evident that this 17 nm radius NW does not undergo plastic deformation and undergoes an abrupt fracture event at a critical load (F_{cr}) of 1106 nN. The ultimate strength of the material can then be computed as[10]

$$\sigma_{ult} = \frac{F_{cr}L_{NW}}{2\pi R_{NW}^3} g(\alpha), \tag{2}$$

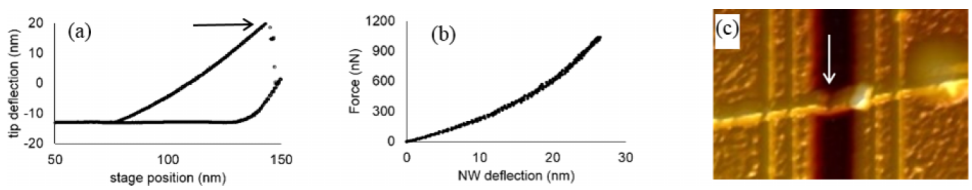

FIG. 4. (a) The AFM loading and unloading curves of a NW device, which exhibited brittle fracture. The arrow indicates the onset of fracture. (b) The extracted force vs. displacement plot, shown here up to the fracture point. (c) An AFM image of the post-fracture NW device with the arrow pointing to the fracture location. The ultimate strength of this NW is calculated as 10.9 GPa.

where $g(\alpha) = \frac{4}{\sqrt{\alpha}} \tanh\left(\frac{\sqrt{\alpha}}{4}\right) + \sqrt{\left(\frac{2+\cosh\left(\sqrt{\alpha}/2\right) - \frac{6\sinh(\sqrt{\alpha}/2)}{\sqrt{\alpha}}}{\alpha\cosh^2\left(\sqrt{\alpha}/4\right)}\right)}$. From the above equation, the ultimate strength of the [111] Ge NW was calculated to be 10.9 GPa. This experimental value represents ~74.5% of the predicted theoretical strength (of $E/2\pi$,[25] or 14.6 GPa) for this NW material. In prior work, theoretical-to-experimental ultimate strength ratios of ~50% and 88% have been reported for Si[26,27] and [112] Ge NWs,[10] respectively. Our measurement is at the higher end of this reported range for the experimental-to-theoretical strength ratio and indicates a relatively defect-free NW crystal.

We have presented the YM measurements from [111] Ge NWs, which were obtained using the AFM based three-point bending technique. The observed average value of 91.9 GPa is lower than the theoretical value for this crystal due to the presence of an amorphous oxide layer. When the softer oxide surface layer is accounted for using a core-shell model, the average YM of the intrinsic Ge core is calculated to be 147.6 GPa, which approaches the theoretical value for [111] Ge. Our results point to the significance of these relatively thin surface layers on the effective elastic properties of nanostructured material systems. This aspect, which has not been addressed so far within the mathematical models that are being used today, needs to be suitably accounted for while predicting the lithiation-induced stress-fields and fracture in these promising new material systems. It is important to note that the surface oxide has previously been shown to have beneficial effects in one-dimensional silicon anodes by preferentially directing the dimensional volume expansion during the lithiation process and thereby stabilizing the solid electrolyte interphase layer.[28] Hence, we would like to emphasize that our observation points only to the importance of accounting for the impact of this surface oxide layer on the elastic properties of the NW and does not necessarily entail a conclusion/recommendation to preferentially eliminate them, which may be possible using chemical etching techniques involving HF or HCl acids. Furthermore, our results point to an exceptionally high experimental-to-theoretical ratio for the ultimate strength of these crystals. This is another important attribute that advances their suitability for use as high-capacity and high-rate alloying anode systems in next-generation batteries.

This work was partly supported by the National Science Foundation under Grant No. 1453966. This work was performed, in part, at the Sandia-Los Alamos Center for Integrated Nanotechnologies (CINT), a U.S. Department of Energy, Office of Basic Energy Sciences user facility. This involved chip nanofabrication activities at CINT, which were performed under the user Proposal No. U2014A0084. Sandia National Laboratories is a multi-program laboratory operated by Sandia Corporation, a wholly owned subsidiary of Lockheed Martin company, for the U.S. Department of Energy's National Nuclear Security Administration under Contract No. DE-AC04-94AL85000.

[1] C. K. Chan, H. Peng, G. Liu, K. McIlwrath, X. F. Zhang, R. A. Huggins, and Y. Cui, Nat. Nanotechnol. **3**, 31 (2008).
[2] C. K. Chan, X. F. Zhang, and Y. Cui, Nano Lett. **8**, 307 (2008).
[3] T. Kennedy, E. Mullane, H. Geaney, M. Osiak, C. O'Dwyer, and K. M. Ryan, Nano Lett. **14**, 716 (2014).
[4] F.-W. Yuan, H.-J. Yang, and H.-Y. Tuan, ACS Nano **6**, 9932 (2012).
[5] D. Wang, Y.-L. Chang, Q. Wang, J. Cao, D. B. Farmer, R. G. Gordon, and H. Dai, J. Am. Chem. Soc. **126**, 11602 (2004).
[6] J. Graetz, C. C. Ahn, R. Yazami, and B. Fultz, J. Electrochem. Soc. **151**, A698 (2004).
[7] S. W. Lee, I. Ryu, W. D. Nix, and Y. Cui, Extreme Mech. Lett. **2**, 15 (2015).
[8] J. Park, W. Lu, and A. M. Sastry, J. Electrochem. Soc. **158**, A201 (2011).
[9] D. A. Smith, V. C. Holmberg, D. C. Lee, and B. A. Korgel, J. Phys. Chem. C **112**, 10725 (2008).
[10] L. T. Ngo, D. Almecija, J. E. Sader, B. Daly, N. Petkov, J. D. Holmes, D. Erts, and J. J. Boland, Nano Lett. **6**, 2964 (2006).
[11] B. Varghese, Y. Zhang, L. Dai, V. B. C. Tan, C. T. Lim, and C.-H. Sow, Nano Lett. **8**, 3226 (2008).
[12] H. Ni, X. Li, and H. Gao, Appl. Phys. Lett. **88**, 043108 (2006).
[13] B. Wen, J. E. Sader, and J. J. Boland, Phys. Rev. Lett. **101**, 175502 (2008).
[14] B. R. Burg, V. Bianco, J. Schneider, and D. Poulikakos, J. Appl. Phys. **107**, 124308 (2010).
[15] A. Subramanian, T. Choi, L. X. Dong, J. Tharian, U. Sennhauser, D. Poulikakos, and B. J. Nelson, Appl. Phys. A **89**, 133 (2007).
[16] A. Subramanian, N. S. Hudak, J. Y. Huang, Y. Zhan, J. Lou, and J. P. Sullivan, Nanotechnology **25**, 265402 (2014).
[17] N. K. R. Palapati, E. Pomerantseva, and A. Subramanian, Nanoscale **7**, 3109 (2015).
[18] J. E. Sader, J. W. M. Chon, and P. Mulvaney, Rev. Sci. Instrum. **70**, 3967 (1999).
[19] A. Subramanian, A. R. Alt, L. X. Dong, B. E. Kratochvil, C. R. Bolognesi, and B. J. Nelson, ACS Nano **3**, 2953 (2009).
[20] E. Borchi, S. D. Gennaro, R. Macii, and M. Zoli, J. Phys. D: Appl. Phys. **21**, 1304 (1988).
[21] J. J. Wortman and R. A. Evans, J. Appl. Phys. **36**, 153 (1965).
[22] A. J. Lee, M. Kim, C. Lena, and J. R. Chelikowsky, Phys. Rev. B **86**, 115331 (2012).

[23] C. Q. Chen, Y. Shi, Y. S. Zhang, J. Zhu, and Y. J. Yan, Phys. Rev. Lett. **96**, 075505 (2006).
[24] S. Spinner and G. W. Cleek, J. Appl. Phys. **31**, 1407 (1960).
[25] C. R. Barrett, W. D. Nix, and A. S. Tetelman, *The Principles of Engineering Materials* (Prentice Hall, Englewood Cliffs, NJ, 1973).
[26] S. T. Boles, A. Sedlmayr, O. Kraft, and R. Monig, Appl. Phys. Lett. **100**, 243901 (2012).
[27] S. Hoffman, I. Utke, B. Moser, J. Michler, S. H. Christiansen, V. Schmidt, S. Senz, P. Werner, U. Gosele, and C. Ballif, Nano Lett. **6**, 622 (2006).
[28] H. Wu, G. Chan, J. W. Choi, I. Ryu, Y. Yao, M. T. McDowell, S. W. Lee, A. Jackson, Y. Yang, L. Hu, and Y. Cui, Nat. Nanotechnol. **7**, 310 (2012).